# R2S 2026 Critical Design Report

BristolSEDS Experimental Propulsion

# Table of Contents

***Note: BSEP is the propulsion arm of HyPower Bristol which is a subsidiary of BristolSEDS, the University of Bristol's branch of SEDS (Students for the Exploration and Development of Space). All 3 names can be used for the team interchangeably.***

# Part A

## A1 – Project Introduction

This document is the Critical Design Report for BristolSEDS Experimental Propulsion's (BSEP) 2026 R2S entry. Building upon the successful 5 kN design architecture established during the previous cycles, this year's mission aims to refine the system for higher performance. While the overarching goal remains a regeneratively cooled, additively manufactured engine producing 5kN of thrust, the 2026 mission introduces a significant technical leap with the team's first transition to Liquid Oxygen as the oxidizer.

Due to lessons learned during previous hotfire and integrated tests, the team has transitioned back to Inconel 718. With the ultimate goal of flying this Engine in the 9km liquid category at the European Rocketry Challenge (EuRoC) 2027, this material choice allows us to push the engine to its efficiency limits without having to worry about the fragility of Aluminium-based alloys in off-nominal scenarios that are inherently possible during integrated flight testing (such as ox-rich shutdowns).

The main innovation of this project lies in our shift to an "Ox-Centered Swirler" injector design. In a departure from previous fuel-centered architectures, this new design utilizes oxidizer injection through the central swirl element while fuel is injected through the outer stage. This configuration simplifies the manifold architecture, enhances mixing, and permits the removal of traditional film cooling to increase overall efficiency. New simulation methods will be developed to characterize and validate the novel swirler geometry as well as its effects on inner chamber wall thermals.

The R2S competition provides a platform to validate the performance of the engine and injector as well as give the team the opportunity to gain experience with cryogenics before moving towards a full launch vehicle.

## A2 – Engine Design Overview

The BSEP Engine-4 is a high-efficiency, regeneratively cooled bi-propellant liquid rocket engine designed for a 5kN thrust target with an 8-second design burn time. The engine operates at a nominal chamber pressure of 20 bar using Liquid Oxygen (LOx) and Isopropyl Alcohol (IPA) as propellants.

The chamber is designed for additive manufacture using Inconel 718 to ensure maximum structural reliability under the extreme thermal loads of LOx combustion. Thermal management is primarily achieved through an opposite-flow regenerative cooling. IPA fuel circulates through 48 spiral cooling channels oriented at a 35° angle to the generatrix before reaching the injector plate.

The engine utilizes a co-axial swirl injector in an oxidizer-centred configuration. In this arrangement, LOx passes directly from the top of the engine into the inner swirlers, while the fuel enters the outer swirlers from the regenerative cooling channels.

The engine dimensions remain compatible with existing BSEP hardware to ensure seamless integration into existing launch vehicle systems and to continue to allow all BSEP chamber and injectors to be interchangeable. This allows for the use of a backup engine (Engine 1) in the event that Engine 4 is not manufactured by the required deadline. The necessary simulations and calculations for both engines are detailed within this document.

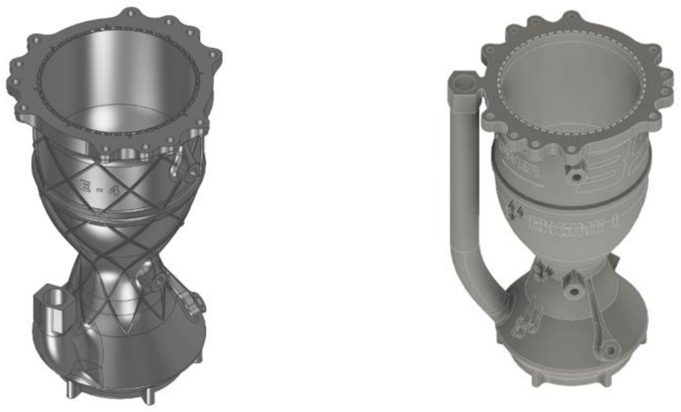

(a) (b)

*Figure 1: Full chamber CAD of (a) Engine-4 and (b) Engine-1*

## A3 – Engine Parameter Table

*Table 1: BSEP engine parameters*

| Parameter | Data | Unit |
|---|---|---|
| Propellants | IPA and LOx | $n/a$ |
| Cooling Used | Regenerative, Film | $n/a$ |
| Desired Fuel Mass Flow | 0.828 | $kg/s$ |
| Desired Ox Mass Flow | 1.325 | $kg/s$ |
| OF Ratio | 1.6 | $n/a$ |
| Port Connectors (Injector) | Ox: 3/4" BSPP | $n/a$ |
| Port Connectors (Cooling) | Fuel: 1/2” BSPP (regen) | $n/a$ |
| Design Thrust | 5.0 | $kN$ |
| Design Burn Time | 8.0 | $sec$ |
| Desired Fuel Delivery Pressure | 30 | $bar$ |
| Desired Ox Delivery Pressure | 30 | $bar$ |
| Designed Chamber Pressure | 20 | $bar$ |
| Ignition System | Airborne Torch Igniter | $n/a$ |

# A4 – Engine Description

## A4.1 – Combustion Chamber

Two combustion chambers have been designed and simulated, with the aim of testing only <u>one</u> at R2S 2026. Both engines have the same engine parameters, material (Inconel 718), and similar geometry due to their interoperability with the injector.

### *A4.1.1 – Engine-4*

"Engine-4" is the new engine designed for the R2S 2026 competition. It is a regeneratively cooled constant angle spiral channel engine with mass saving design features (isogrid). The details of this engine are listed in the figures [] and table [] below.

*Table 2: Engine-4 dimensions*

| Property | Value |
|---|---|
| Engine length | 281.0mm |
| L* | 839.4mm |
| Chamber diameter | 117.8mm |
| Throat diameter | 48.10mm |
| Expansion area ratio | 3.81 |
| Contraction area ratio | 6.00 |

*Table 3: Engine-4 cooling channel dimensions*

| Property | Value | Units |
|---|---|---|
| Wall thickness | 0.8 | $mm$ |
| Number of cooling channels | 48 | [-] |
| Rib thickness 'b'<br>*(Chamber - Throat - Manifold)* | 1.00 – 0.90 – 1.10 | $mm$ |
| Channel width 'a'<br>*(Chamber - Throat - Manifold)* | 4.00 – 2.00 – 3.00 | $mm$ |
| Channel height 'hc'<br>*(Chamber - Throat - Manifold)* | 2.00 – 2.00 – 2.00 | $mm$ |
| Channel angle | 35.0 | ° |

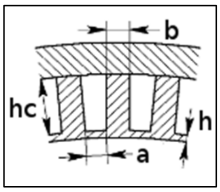


*Figure 2: Cooling channel cross section & labels*

## A4.2 – Injector

### *A4.2.1 - Summary*

This year we have iterated on our R2S '25 injector, retaining the coaxial-swirl injection scheme. However, there are a number of key differences: the switch to Liquid Oxygen (LOx) has facilitated a move to 'fuel external' swirlers – see Figure 3 (left) – due to the lower O/F and its higher density. This also simplifies manifold positioning, as the fuel entering the injector from the regenerative cooling channels can be directly transferred to the lower fuel manifold, rather than having to be moved over the oxidiser manifold – see Figure 3 (right). This manifold simplification also allows for a reduction in the total number of seals, whilst the number of inter-propellant seals remains zero.

### *A4.2.2 – Injection Scheme Details*

Much like last year there are five co-axial swirl elements on the injector plate, each identical and designed using Bazarov's methods (See A8.1 – Injector Sizing for more information on swirler design). These were chosen due to their excellent atomisation allowing for performance close to the theoretical maximum. The injector also does not incorporate film cooling to maximise efficiency.

### A4.2.3 – Manifold Scheme Details

The injector has two manifolds, the lower one feeds the outer fuel swirlers whilst the upper supplies the inner oxidiser swirlers. All have instrumentation ports to allow for the determination the fluid temperature and manifold pressure.

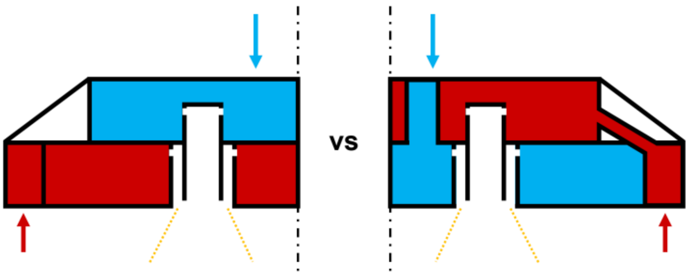


*Figure 3 - Comparison of Fuel External (left) and Ox External (right) Swirler Designs*

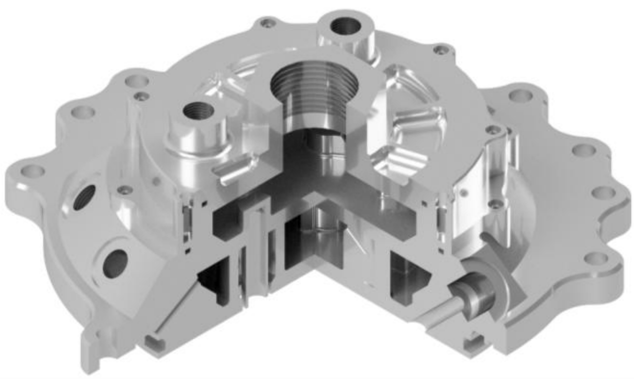

*Figure 4 - 3/4 Section of the Injector Plate*

Oxidiser is supplied to the injector through a 3/4" BSPP Port in the centre of the injector's top plate. For a full breakdown of the ports please consider the diagram below:

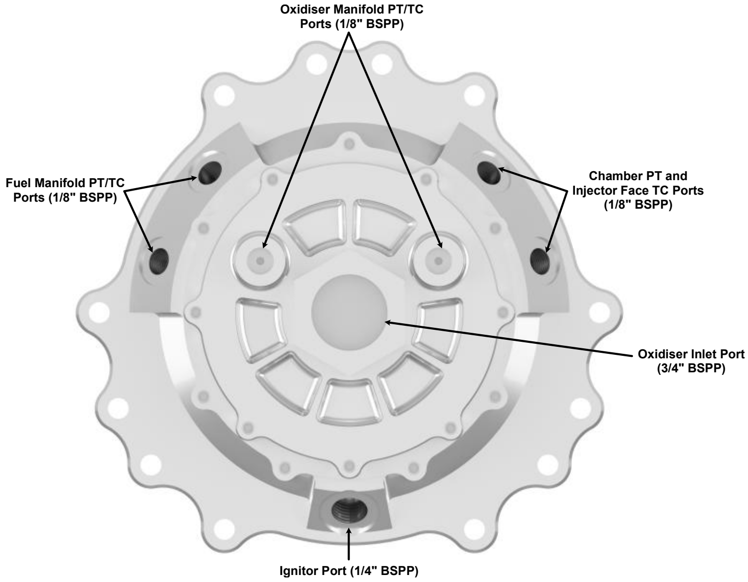


*Figure 5 - Injector Port Diagram*

## A4.3 – Seals & Interfaces

As the engine is pre-chilled all the seals on it must be able to withstand cryogenic temperatures. There are a very limited number of materials that can operate in such harsh environments, prime amongst them is PTFE/PCTFE which has an operating temperature for O-Rings all the way down to around $-200\,°C$. The table below shows the selected seals for the injector plate, and its interfaces with the combustion chamber.

*Table 4 - Injector Seals Information*

| Seal Name | Material | Dimensions |
|---|---|---|
| Combustion Chamber Piston Seal | Silicone (VMQ) | 110.7x3.53mm |
| Fuel Pickup Face Seal | PTFE | 133.07x1.78mm |
| Fuel Manifold Face Seal | PTFE | 94.97x1.78mm |
| Oxidiser Manifold Face Seal | PTFE | 82.27x1.78mm |

All of the face seals on the injector plate will be PTFE O-Rings, which are capable of withstanding cryogenic temperatures, whilst the piston seal is a silicone elastomeric O-Ring – chosen for its low temperature performance (albeit not as good as PTFE).

We initially intended the piston seal with the chamber shall be a spring energized seal manufactured by Parker part number: YT60324TE009. However, there were significant costs to spring energized seals, primarily in the MOQ rather than each individual seal being too expensive. As a result, we have had to revert to standard elastomeric O-Ring seals for the chamber piston seal to maintain backwards compatibility of the engine with older injector plates. These are not rated for cryogenic service, so calculations were completed to calculate the potential leakage of the unsealed gap in the worst-case scenario.

The tolerance for injector plate manufacturing is -0.1mm with the chamber I/D of 119.6mm meaning that we have an effective gap width of 0.1mm and O/D 119.6 with I/D of 119.5, giving an effective leak area of 18.78mm$^2$. Which assuming a $C_d$ of 0.6, a $\Delta P$ of 10 bar, and idealising as a sharp-edged orifice would result in a leak rate of 0.4467 kg/s – approximately half of our desired fuel mass flow rate. It should be noted that this is a 'safe leak' as we are introducing fuel to the walls of the chamber which will cool the combustion as well as the fact that it assumes the O-Ring has completely failed and doesn't contribute to blockage, as well as not taking into account the relative thermal expansion of the steel injector plate vs the Inconel combustion chamber. The final point is especially important as stainless steel's thermal expansion coefficient is around 50% higher than Inconel 718's whilst also possessing a higher thermal conductivity. All of this combined means that the size of the gap between the injector plate and the combustion chamber wall will be smaller than expected, as the injector plate will expand more and more quickly than the combustion chamber.

In addition to the injector seals, we must also consider the fittings and their seals, as Dowty washers are inoperable at cryogenic temperatures. As a result, all of the Swagelok fittings must be sealed using copper gaskets.

The diagram below shows the seal arrangement for the Injector Plate:

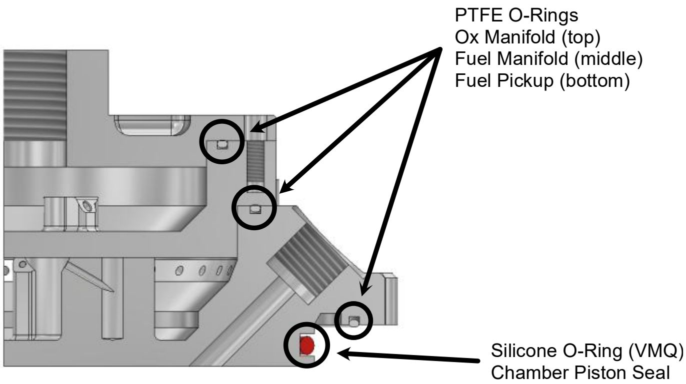


*Figure 6 - Seal Arrangement Diagram*

## A5 – Project Management

Financial support for the project is secured through a combination of BristolSEDS grants and Hypower internal budget allocations, which are bolstered by a diverse portfolio of society-and-team-wide cash sponsorships. The manufacturing phase is currently underway as the injector assembly is scheduled for submission to the machine shop by the end of April, with an anticipated completion date in late May. While the 3D-printing schedule for Engine-4 is currently unconfirmed, this does not present a risk to the primary mission timeline as Engine-1 remains fully viable and hotfire-ready, serving as a qualified backup to ensure project continuity.

# A6 – Testing Plan Overview

The test outlines below are preliminary and subject to change following input from test facility and future potential design changes. Integration with the test facility at Airborne Engineering Ltd is facilitated by the ICD provided by the Race to Space competition.

Commented [ES1]: ethan make this more glamorous

## A6.1 – Test 1: Full duration Burn 1

Commented [TW2]: @Ethan Sheehan You need to update the tests

A full duration burn to act as a benchmark for thrust and chamber pressure. 8 seconds was chosen to put us at the EuRoC impulse limit and is the burn time we would use for a 9km launch vehicle.

*Table 5: Test parameters for full duration burn hotfire*

| Property | Test Value | Unit |
|---|---|---|
| Oxidiser injector feed pressure | 30 | $bar$ |
| Fuel injector feed pressure | 30 | $bar$ |
| IPA mass flow | 0.864 | $kg/s$ |
| LOx mass flow | 1.296 | $kg/s$ |
| OF ratio | 1.5 | $(-)$ |
| Chamber pressure | 20 | $bar$ |
| Thrust | 5 | $kN$ |
| Burn time | 8 | $s$ |
| IPA consumed | 6.912 | $kg$ |
| LOx consumed | 10.368 | $kg$ |

## A6.2 – Test 2: Full duration Burn 2

A second burn to optimize from Test 1 and achieve the nominal values by increasing or decreasing mass flows and pressures as needed to achieve exactly 5kN of thrust.

## A6.3 – Test 3: Depth of Throttle

A long burn starting at half throttle and gradually throttling down to determine the depth of throttle of the injector.

## A6.4 – Test 4: Increased Chamber Pressure

Dependent on the thermal data results from Test 1 & 2, propellant feed pressures will be increased to test the limits of the engine's performance. Calculations will be able to be performed on the spot to confirm the engine could still survive the increased pressure with a 1.2× safety factor.

# A7 – Planned Instrumentation

Multiple thermocouple ports are built into the chamber and pressure transducer ports are built into the injector to allow collection of sensor data. A series of wet and dry thermocouples are used to monitor the temperature of coolant along the channel walls, and a pair of pressure transducers are present on the injector to log the incoming pressure of the fuel and as well as the chamber pressure in the engine. The figure below lays out the sensor arrangement for the engine. From injector-face to nozzle, sensors are labelled based on their column and row. This allows for the unique labelling of each sensor when designating and data logging/graphing.

Commented [TW3]: @Ethan Sheehan You also need to change the text in all of these sections to Arial

*Table 3: Key instrumentation properties*

| Type | Value | Range | Part | Connection |
|---|---|---|---|---|
| Temperature | T(XX) | 198 – 523 K | T type thermocouple | Type T Connection |

| | | | | |
|---|---|---|---|---|
| Pressure | P(XX) | 0 – 60 Bar | GPT200 Universal | 4 pin M12 |


*Figure 7: Instrumentation diagram*

# A8 – Design Calculations

## A8.1 – Injector Sizing

*Table 6: Injector geometry nomenclature*

| Variable | Definition |
|---|---|
| $D_n$ | Diameter of the nozzle |
| $R_s$ | Radius of the swirl chamber |
| $r_{in}$ | Radius of the inlet to the swirl chamber |
| $l_s$ | Length of the swirl chamber |
| $l_n$ | Length of the nozzle |
| $\beta$ | Angle of contraction of the inner wall |

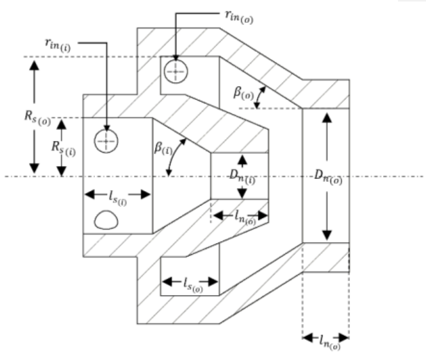

Using the methodology found in B3.1 – Swirl Element Sizing Method, and an in-house script to iterate it, we obtain the inner oxidiser swirl element dimensions to be:

*Table 7: Oxidiser swirl element properties & dimensions*

| Property | Value | Unit |
|---|---|---|
| Oxidiser mass flow | 0.43 | $kgs^{-1}$ |
| Oxidiser nozzle diameter | 6.8 | $mm$ |
| Oxidiser vortex chamber diameter | 12 | $mm$ |
| Oxidiser Inlet Port Size | 3 | $mm$ |
| Oxidiser Fan Angle | 120 | ° |

The fuel swirlers were sized to the minimum diameter swirl element with 1 mm air gap clearance to the inner swirl element's nozzle wall as the dimensional limit.

## A8.2 – Chamber Stress Calculations

A series of analytical and computational simulations were performed to validate the stress experienced by each part of the system.

### *A8.2.1 – Material Properties*

The tabulated material properties detailed in Table 8 were provided by the material supplier and printing company, the MTC.

*Table 8: Material properties of Inconel 718 used within chamber stress calculations*

| Property | Value | Unit |
|---|---|---|
| Melting Point | 1500 | $K$ |
| Maximum Operating Temp (MOT) | 1050 | $K$ |
| Yield Strength | 1172 | $MPa$ |
| Yield Strength at MOT | ~758 | $MPa$ |
| Thermal Conductivity | 18 | $W/m \cdot k$ |
| Thermal Conductivity at MOT | 22.0 | $W/m \cdot k$ |
| Young's Modulus | 208 | $GPa$ |
| Young's Modulus at MOT | 130 | $GPa$ |
| Poisson Ratio | 0.31 | [--] |
| Thermal Expansion Coefficient | $16.0 \times 10^{-6}$ | $°C^{-1}$ |

### *A8.2.2 – Chamber Stress Analysis*

The stress results at every point along the engine contour were calculated using the equations in Appendix B3.3 The tangential stresses were split into their hoop and thermal parts as well as combined. The yield strength values were extrapolated to accurately model when they will yield in each location at the operating temperature that location will experience.

**Engine-4**

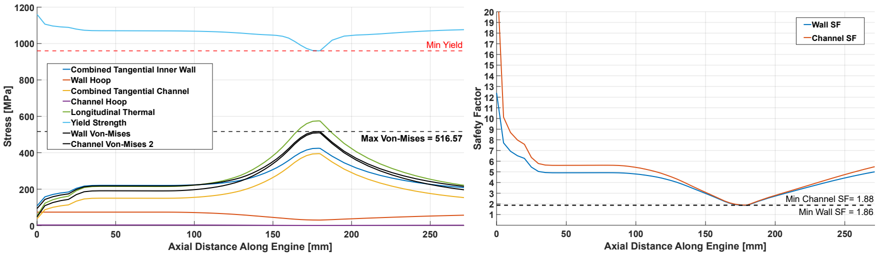


| Property | Value |
|---|---|
| Minimum wall safety factor | 1.88 |
| Minimum channel safety factor | 1.86 |
| Maximum von-Mises stress | 516.57 $MPa$ |

### *A8.2.4 – Stress Considerations*

The above simulations demonstrate the "worst-case scenario" for the performance of the combustion chambers. Consideration should be given to the fact that the following beneficial factors have not been included in this modelling due to the difficulties involved in integrating these features:

- The Bartz equation has been used which is known to overestimate when compared to other sources such as the Levlev equation and empirical data.
- The effects of PDMS were not simulated. The addition of 2% PDMS to the fuel will act to considerably decrease wall temperatures (~20% heat flux reduction) at hotspots such as the throat and hence increase various material properties such as the tensile and yield strength.

As the analysis capabilities mature each of these features will be included, increasing the confidence in the stress and thermal simulations.

## A8.3 – Chamber Thermal Analysis

Cooling strategies were converged upon though a series of thermal and mechanical stress simulations. Rocket Propulsion Analysis (RPA) was used to implement the Bartz equation for heat transfer coefficient through the chamber and nozzle boundary layer. Hot wall temperatures were then inserted into a thermal hoop stress calculation to derive stress values which fed redesign of thermal solutions until a final solution was converged upon. Additionally, a 10% film cooling solution was added to further reduce the thermals reached by the engine and a 2% addition of the additive PDMS will further reduce temperatures at hotspots.

The graphs (Figure 8, Figure 22) and tables (Table 9, Table 13) below display the results of the thermal simulations without the simulated use of PDMS where $Twi$ is the inner wall temperature chamber, $Twc$ is the inner wall temperature of the cooling channels, and $Tc$ is the temperature of the coolant. The graph demonstrates that even without factoring in the effects of PDMS the operating temperatures of both chambers are below the maximum recommend operating temperature of Inconel 718 (1050K) at all points along the engine.

**Engine-4**

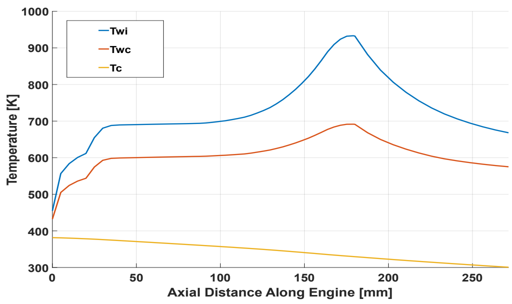


*Figure 8: Engine 4 temperature profile (without PDMS)*

*Table 9: Key thermal values for Engine-4*

| Property | Value | Units |
|---|---|---|
| Maximum chamber-side wall temperature | 933 | $K$ |
| Maximum coolant-side wall temperature | 691 | $K$ |
| Maximum coolant temperature | 381 | $K$ |
| Minimum velocity of coolant | 3.88 | $ms^{-1}$ |
| Maximum heat flux | 5437 | $kWm^{-2}$ |
| Increase in coolant temperature | 83 | $K$ |

## A8.4 – Bolt Calculations

A pattern of 12 M6 bolts has been included to secure the injector into the combustion chamber as well as to mount the chamber to the rocket itself. Half of the 12 bolts will be used for mounting the injector plate to the combustion chamber. From basic static equilibrium:

$$\sigma_b = \frac{P_c * A_I}{N_b * A_b} = \frac{20\ bar * \pi(0.0598)^2}{6 * 20.1 * 10^{-6}} = 186.3\ MPa \tag{1}$$

Where, $\sigma_b$ is the stress on each bolt, $P_c$ is the nominal chamber pressure, $A_I$ is the circular area of the injector face exposed to the chamber pressure, $N_b$ is the number of bolts exclusively in use to attach the chamber to the injector, and $A_b$ is the tensile stress area of an M6 coarse pitch thread bolt. Considering a safety factor:

$$SF = \frac{\sigma_{yield\ of\ ISO\ Grade}}{\sigma_b}$$

With ISO Metric Bolt Grades of 4.6 and 10.9, the safety factors achieved are 1.29 and 5.05, respectively.

## A8.5 – L-Bracket

Mounting is achieved using an aluminium mounting plate. This will transfer loads from the engine to the test stand. The same setup was proven highly effective in previous hot-fires of similar thrust. The full setup is seen below in Figure 7.

The engine mount, which interfaces with the test stand, is constructed out of 10mm plate aluminium with bolted interfaces for ease of assembly and disassembly. The L-bracket's structural performance was evaluated through Finite Element Analysis. A 5kN nominal thrust force was loaded at the contact surface between the engine mount and engine, assuming rigid bolt connections. This resulted in a maximum displacement and Von misses stress of 0.51mm and 52.52MPa respectively (safety factor of 5), indicating that the L-bracket can sustain loads substantially larger than the nominal design thrust.

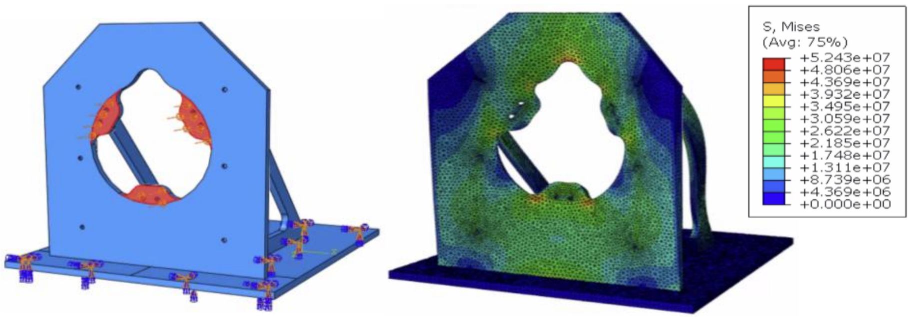


*Figure 9: Finite Element Analysis of the L-bracket (deformation scale factor of 85).*

The engine mount is to be fastened to the available thrust plate as specified by the Airborne Engineering Ltd J1 test site via 16xM10 and the BSEP engine via 6xM6 bolts. The bottom face mounting plate can be drilled to fit the requirements of the test stand in question.

### 8.4.1 – L-Bracket Bolt Calculations

Taking nominal thrust to be 5kN and given the maximum stress of the L-Bracket is 52.52MPa, the maximum shear stress per bolt on the bolts holding the L-Bracket to the thrust plate can be calculated using the following equation:

$$\tau_{bolt} = \frac{F_{engine}}{NA_{bolt}}$$

Here, $\tau_{bolt}$ is the maximum shear stress on a single bolt, $F_{engine}$, $N$ is the number of bolts and $A_{bolt}$ is the cross-sectional area of the bolt (assuming shear plane passes through the unthreaded shank). Evaluating this equation gives a maximum shear stress of 3.97MPa. This value can be compared to an existing bolt such as the 12.9 grade Socket Cap heads from

Trident Racing Supplies, which has a shear strength of 517MPa. Therefore, we find that the bolts are sufficient to hold the L-bracket in place with a safety factor large enough to handle the added loads associated with a hardstart. Additionally, the thrust force will be distributed across the L-bracket so it is extremely unlikely that the bolts will experience the maximum stress, giving an added layer of confidence that the bolts are adequate.

#### 8.4.2 – Engine Mount Bolts

The following bolt pattern was chosen to hold the engine in the mount:

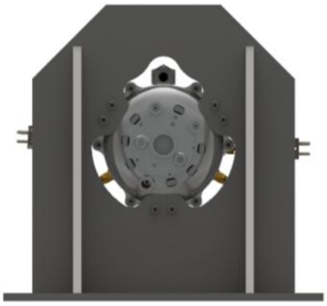

*Figure 10: Bolthole locations within L-bracket*

Three sets of two bolts were chosen to hold the engine in the L-bracket at equal intervals. Slots would also be cut to account for the pipes to attach to the mount. The bolts will go through the holes in the engine, injector plate and L-Bracket as shown in the top view CAD below:

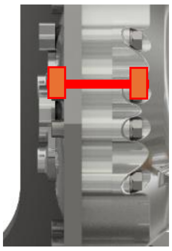

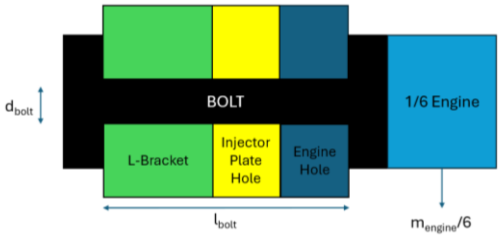


*Figure 11: Bolt location highlighted on CAD (left). Schematic to describe assemble around bolt (right).*

## A8.6 – Inlet Velocities

The inlet velocities for the Fuel and Oxidiser can be simply calculated using the flow rate equations:

$$Q = Av$$

Where $Q$ is the volumetric flow rate, $A$ is the cross-sectional area, and $v$ is the average fluid velocity. We can rearrange this equation and substitute to obtain:

$$v = \frac{Q}{A} = \frac{\dot{m}}{A\rho}$$

Where $\rho$ is the density of the fluid, and $\dot{m}$ is the mass flow rate. We can therefore calculate the inlet velocities for the fuel and oxidiser ports using:

*Table 10: Fuel and oxidiser inlet properties*

| Fluid | $\dot{m}\ (kg/s)$ | A $(m^2)$ | $\rho\ (kg/m^3)$ | Velocity $(ms^{-1})$ |
|---|---|---|---|---|

| | | | | |
|---|---|---|---|---|
| IPA | 0.86 | $6.9 \times 10^{-5}$ | 786 | 15.86 |
| LOx | 1.29 | $1.7 \times 10^{-4}$ | 1141 | 6.65 |

# Part B

## B1 – Positionality Statement

This year marks BristolSEDS Experimental Propulsion's 4th engine design and third entry into Race 2 Space. It builds upon BSEP's experience in liquid propulsion while incorporating new challenges for the team to face.

Engine-1 was originally designed for R2S 2024 by a small team of 5 members and was the University of Bristol's first every student built liquid rocket Engine. The design featured a 5kN regeneratively cooled AM Inconel 718 combustion chamber and a steel like-like impinging NOS/IPA injector. Due to a series of complications with the original print, the team was unable to test during the competition. With support from the Manufacturing Technologies Catapult, the team later received the chamber and were able to hotfire test the engine on January 10, 2025, at Airborne Engineering Ltd. Three successful tests were conducted, pushing the chamber 20% past its design thrust to 6kN, being the first student team in the UK to break 5kN of thrust and claiming the UK student thrust record at the time.

Engine-2 was designed for R2S 2025 and for HyPower's EuRoC '25 3km launch vehicle. This was a flight-weight iteration of Engine-1, utilizing CP-1 Aluminium for the combustion chamber and an aluminium coaxial swirl NOS/IPA injector plate. This was the first time the CP1 alloy had ever been used for a rocket engine. The engine was hotfired at R2S 2025, but due to swarf in the cooling channels introduced during post-machining, did not have a nominal burn. Because of the swarf clogging the fuel orifices, almost no IPA was able to flow through cooling channels and through the injector, removing the regenerative, film, and additive cooling effects from the PDMS. This complete lack of cooling caused the combustion chamber to fail in multiple locations. Nevertheless, this was an extremely interesting result and the team collected lots of data and lessons learned. The fact the engine fired under these conditions and achieved 2.1kN was a major success and validated the robustness of the swirler design. A steel H2/O2 torch ignitor was also tested at Astron Systems during R2S 2025, achieving 10 firings before melting.

Since the combustion chamber for Engine-2 was destroyed, the propulsion flight qualification campaign for HyPower's EuRoC '25 launch vehicle used Engine-1 instead. In September 2025, three integrated hotfires were successfully conducted at Astron System's facility using BSEP's SRAD feed system and tanks, qualifying the vehicle for flight and allowing the team to pass the Flight Readiness Review.

Engine-3 was designed as a replacement for the destroyed Engine-2, featuring an improved CP-1 chamber with spiral cooling channels which should decrease the inner wall temps by 10%. This engine will be used on HyPower's EuRoC 26' launched vehicle.

## B2 – Mission Statement

Race 2 Space serves as an integral part of the test & development cycle for HyPower Bristol. HyPower Bristol has entered EuRoC yearly, competing in the liquid 3km category for 2024 and 2025. In 2026, we aim to launch a nitrous oxide and ethanol fuelled rocket to 9km. Without the facilities and expertise provided by Race 2 Space, the development and launch of a flight-optimised liquid rocket would be significantly more challenging.

Looking forward, the team is aiming to switch to a LOx based propellant rocket, also targeting 9km. This launch vehicle design will be primarily informed from data collected during R2S 2026 and will set the foundation for HyPower to aim for higher targets. Race 2 Space provides HyPower Bristol with a structured, repeatable environment to develop our propulsion system.

## B3 – Appendices

### B3.1 – Swirl Element Sizing Method

We use Bazarov's method from "Design and Dynamics of Jet and Swirl Injectors" to design elements which we are not simulating (i.e. the Ox Swirlers on this year's injector plate). This method follows:

Two pertinent design procedures are outlined by Bazarov: a single mono-propellant swirl injector (often referred to as a "simplex"), and the combination of two mono-propellant swirl injectors to form a coaxial swirl injector.

Single Swirler

1)

Prescribe the spray cone half angle (i.e. half the total fan angle), and determine both the geometric characteristic $A$ and the flow coefficient $\mu$ from the plot:

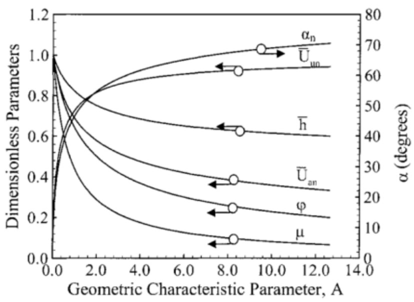


*Figure 12 — Effects of A on other injector parameters*

2)

Determine the nozzle radius using,

$$R_n = \frac{1}{\sqrt{\pi\sqrt{2}}}\sqrt{\frac{\dot{m}_i}{\mu\sqrt{\rho\Delta p_i}}}$$

3)

Specify the number of inlet passages (typically 2 to 4) and $R_{in}$ from geometrical considerations, then the radius of the inlet passage is given by,

$$r_{in} = \sqrt{\frac{R_{in}R_n}{nA}}$$

Where $R_{in}$ is the radial location of the center of the tangential channel, and $n$ is the number of channels.

4)

Determine injector parameters based on the values calculated previously:

- Length of the tangential passages

$$l_{in} = (3\ to\ 6)\ r_{in}$$

- Nozzle length

$$l_n = (0.5\ to\ 2)\ R_n$$

- Vortex-chamber length

$$l_s > 2R_n$$

- Vortex-chamber radius

$$R_s = R_{in} + r_{in}$$

5)

We then find the Reynolds number of the inlet passages using:

$$Re_{in} = \frac{2}{\pi}\frac{\dot{m}_i}{\sqrt{n}r_{in}\rho\nu}$$

Allowing us to calculate the friction coefficient using Blasius correlation:

$$\lambda = \frac{0.3164}{(Re_{in})^{0.25}}$$

6)

We can then find the equivalent area $A_{eq}$ using the equation:

$$A_{eq} = \frac{R_{in}R_n}{nr_{in}^2 + \frac{\lambda}{2}R_{in}(R_{in} - R_n)}$$

Followed by using Figure 12 — Effects of A on other injector parameters) to determine $\mu_{eq}$ and $\alpha_{eq}$.

7)

We can calculate the hydraulic-loss coefficient in the tangential passages using:

$$\xi = \xi_{in} + \lambda \frac{l_{in}}{2r_{in}}$$

Where $\xi_{in}$ is determined from the plot of:

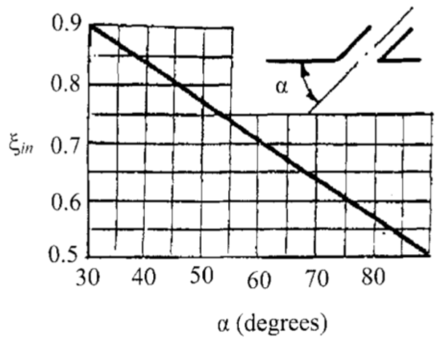


*Figure 13 - Effect of tilt angle of injector passage on coefficient $\xi_{in}$*

Where $\alpha$ (tilting angle of the tangential passage relative to the external surface of the vortex chamber) can be calculated using the equation:

$$\alpha = 90° - \tan^{-1}\frac{R_s}{l_{in}}$$

8)

The actual flow coefficient can then be determined using:

$$\mu_i = \frac{\mu_{eq}}{\sqrt{1 + \xi_i \mu_{eq}^2 \frac{A^2}{\bar{R}_{in}^2}}}$$

Where,

$$\bar{R}_{in} = \frac{R_{in}}{R_n}$$

9)

Which then allows us to obtain a new nozzle radius using the approximation:

$$R_n = \frac{1}{\sqrt{\pi\sqrt{2}}}\sqrt{\frac{\dot{m}_i}{\mu_i \sqrt{\rho \Delta p_i}}}$$

10)

Finally, we can calculate the geometric parameter $A$ in the new approximation:

$$A^{(1)} = \frac{R_{in} R_n^{(1)}}{n r_{in}^2}$$

Steps 1-10 are then repeated until the calculated injector parameters converge.

## B3.2 – Injector Cold Flow Testing

The two schemes of tip mixing and external mixing coaxial swirlers were considered and tested for BSEPS 4th Engine. An example result of our Bazarov implementation is shown below:

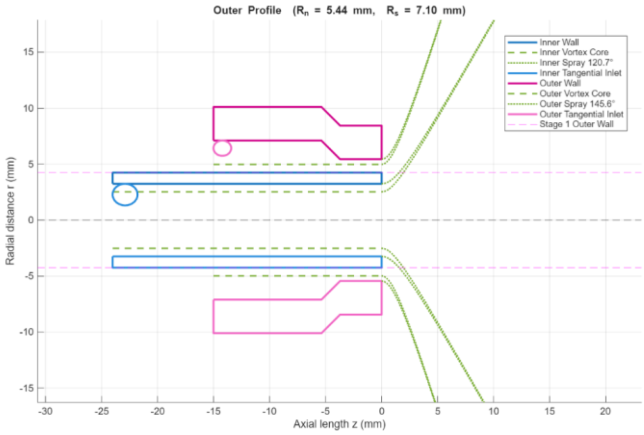


*Figure 17 — Coaxial Tip Mixing scheme with non-impinging fan angles.*

To accommodate the size of the stage 1 inner element in its gas core at the OF ratio and flow rates of Engine – 4, the injector parameters do not converge for larger than 10 – 15 degree differences in fan angles, with the outer fan angle larger than the inner. As a result, in a typical coaxial external mixing setup, impingement does not occur. Through testing of both tip and external schemes, it has been found that at room temperature, 8-15 bar of pressure drop for water, tip mixing schemes mist less than external schemes.

Additionally, the effect of external impingement of the fan angles due to a low-pressure zone in between the two films was observed. As a result, the current considered scheme is an external one.

## B3.3 – Chamber Stress Calculations

### *B3.2.1 – Hoop Stresses*

A series of cases were looked at to determine the hoop stresses experienced by the engine. These simulations verify that the chamber and cooling channel walls will not burst under the pressures they will be subjected to.

***Thick-Walled Hoop Stress***

$$\sigma_\theta = \frac{P_a a^2 - P_b b^2}{b^2 - a^2} + \frac{a^2 b^2 (P_a - P_b)}{(b^2 - a^2) r^2}$$

Lame's equation for thick-walled hoop stress where $\sigma_\theta$ is the hoop stress, $P_a$ is the pressure at the inner surface, $P_b$ is the pressure at the outer surface, $a$ is the inner diameter, $b$ is the outer diameter, and $r$ is the diameter inside the hoop at which the hoop stress is measured.

Multiple cases were tested with different combinations of the 20 bar chamber pressure, 30 bar coolant pressure and 1atm exterior pressure at different thicknesses of the material and point of the engine.

*Table 8: Results for hoop stress calculations.*

| Position | Inner – Outer Pressure [$bar$] | Analytical Value [$MPa$] | Safety Factor (at MOT) |
|---|---|---|---|
| Chamber – Channel | 20 – 30 | 77.8 | 9.7 |
| Chamber – Wall | 20 – 1 atm | 24.4 | 31.0 |
| Throat – Channel | 20 – 30 | 33.8 | 22.4 |
| Throat – Wall | 20 – 1 atm | 10.5 | 72.1 |
| Chamber – Channel | 1 atm – 30 | 224.0 | 3.3 |
| Chamber – Channel | 20 – 1 atm | 150.0 | 5.1 |

Thin wall hoop stress was also used and found to give similar values.

### *B3.2.2 – Thermal Stresses*

Multiple types of thermal stress equations were used as seen below to ensure no cracks or “doghouse effect,” which will be described later, occur. Most of the equations were taken from Stephen D. Heister's “Rocket Propulsion.”

***Tangential Thermal Stress***

Two equations were used to determine tangential thermal stress.

$$\sigma_{t1} = \frac{(P_{co} - P_g)D}{2t} + \frac{E\alpha q t}{2(1-v)k}$$

$$\sigma_{t2} = \frac{(P_{co} - P_g)}{2}\left(\frac{w}{t}\right)^2 + \frac{E\alpha q t}{2(1-v)k}$$

Where $\sigma_t$ is the tangential stress, $P_{co}$ is the coolant pressure, $P_g$ is the combustion gas pressure, $D$ is the chamber diameter, $t$ is the inner wall thickness, $E$ is the Young's Modulus, $\alpha$ is the thermal expansion coefficient, $v$ is the Poisson's ratio, $k$ is the thermal conductivity, and $w$ is the internal width of the cooling channel. Tangential stresses are created by the internal pressure in the coolant passage and its relationship to the local gas pressure as well as due to thermal growth of the material on the heated side of the passage The first half of both equation takes into account the hoop stresses, the first equation calculating it for the inner wall and the second for the channels. The second half of the equation represents the tangential thermal stress induced by heat transfer.

***Longitudinal Thermal Stress***

$$\sigma_l = E\alpha(T_w - T_{ow})$$

Where $\sigma_l$ is the longitudinal stress, $T_w$ is the hot wall temperature, and $T_{ow}$ is the cold wall temperature. The longitudinal stresses result from the tendency of the heated side of the passages to grow in length.

***Thermal Buckling Stress***

$$\sigma_b = \frac{EE_c\frac{t}{D}}{\left(\sqrt{E} + \sqrt{E_c}\right)^2 \sqrt{3(1-v^2)}}$$

Where $\sigma_b$ is the buckling stress and $E_c$ is the compression modulus.

## B3.4 – L-Bracket Drawing

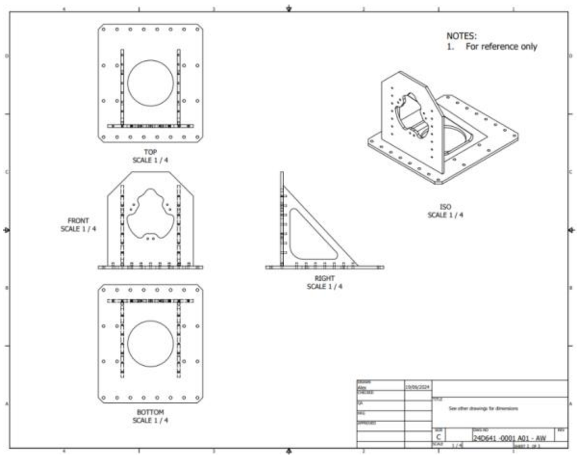


*Figure 14, Drawings for fabrication of L-bracket used to support engine during testing.*

## B3.5 – Engine Mount Bolt Calculations

To verify if bolts will be suitable to hold the engine in place before ignition, a calculation was made with the following simplified diagram, where “1/6 Engine” is a sixth of the lumped mass on the end of a single bolt, since there are six bolts to distribute the load.

Then we can use the bearing stress equation to approximate the load on the bolt:

$$\sigma_{bearing,bolt} = \frac{m_{engine}}{6d_{bolt}l_{bolt}}$$

Assuming the engine mass is 6kg, this will give the bearing stress of 3.7KPa (2.s.f). Compared to the Trident Racing bolt, which has a tensile strength of 1206MPa (Trident Racing Supplies, n.d.), this design would be sufficient. In reality, there would be distributed load along the bolt with considerably more force at the bottom of the bolt towards the engine and the top of the bolt towards on the other side. However, given that the bearing stress is several orders of magnitude below the yield strength, we can conclude it is not necessary to evaluate this stress distribution.

Commented [ES4]: double check these numbers @Tom Wormald

Commented [TW5R4]: I already had Vic do them

## B3.6 – Isogrid Sizing

### *3.6.1 Summary*

The isogrid pattern geometry and smeared elastic properties are derived from the NASA Isogrid Design Handbook (McDonnell Douglas, 1973; NASA contractor report CR-124075). The handbook provides the canonical equations relating rib geometry to an equivalent orthotropic monocoque shell, enabling analytical sizing without a full 3D FEA (Finite Element Analysis), although a FEA was done to correlate results.

### *3.6.2 Pattern Definition*

The Interlocking Helicals pattern is used for the outer wall. It consists of 2 rib families only, both helical at ±55° from the engine axis (subject change for overhang angles for manufacturing). Unlike the full triangular honeycomb isogrid described in NASA CR-124075, this pattern omits the longitudinal (or circumferential) third rib family entirely. The ±55° helix angle is optimal for hoop-dominated loading characteristic of internally pressurised thin-wall shells, providing balanced axial and circumferential stiffness contributions while minimising rib mass.

**Pattern count N** defines the number of starting angular offsets for each helical direction. For N = 4, the pattern consists of 4 clockwise helices and 4 counter-clockwise helices spaced 180° apart, for a total of 4 helical ribs.

### *3.6.3 Helix Path Equations*

A helix of angle α, measured from the engine axis, on a surface of revolution with radius R(x) satisfies the following differential equation:

$$\frac{\mathrm{d}\theta}{\mathrm{d}x} = \frac{\tan(\alpha)}{R(x)}$$

where θ is the circumferential position (radians) and x is the axial coordinate (mm). Integrating from the chamber end:

$$\theta(x) = \int_0^x \frac{\tan(\alpha)}{R(x')}\,\mathrm{d}x'$$

For N starting positions, each helix family is offset by 2π/N radians:

$$\theta_k(x) = \theta(x) + \frac{2\pi k}{N} \quad \text{for k} = 0, 1, \ldots, \mathrm{N} - 1$$

### *3.6.4 2D Unrolled Projection*

The cylindrical surface is unrolled onto a flat rectangle. The horizontal axis is axial position x (mm); the vertical axis is arc length along the circumference, s = R(x)·θ (mm). Each rib path in 3D becomes a curve on this plane. For a constant-radius cylinder this produces straight diagonal lines; for a converging-diverging nozzle, helix paths appear as curves that compress through the throat because the arc length per radian decreases with R.

### *3.6.5 Smeared Equivalent Properties*

For a flanged isogrid with rib width b, web depth d, flange width w_f, flange thickness t_f, and node spacing a, the dimensionless smear ratios are:

$$\alpha = \frac{b\, d}{t\, h}$$

$$\beta = \frac{w_f\, t_f}{t\, h}$$

where h = a·√3/2 is the equilateral triangle altitude and t is the skin thickness. These are NASA Handbook equations 2.1 and 2.2.

The equivalent extensional thickness t* and weight thickness t̄ for the Interlocking Helicals pattern (two rib families, 2/3 of the full isogrid rib count):

$$t^* = t(1 + \frac{2}{3}\alpha + \frac{2}{3}\beta)$$

$$\bar{t} = t(1 + 2\alpha + 2\beta)$$

These reduce to approximately 2/3 of the full triangular honeycomb smear ratios because two helical families carry the load instead of three. The equivalent Young's modulus and bending stiffness follow Handbook equations 2.5 through 2.7.

### *3.6.6 Hoop and Axial Stress (Membrane)*

The pressure load produces membrane stresses on the smeared equivalent shell:

$$\sigma_{\text{hoop}} = \frac{P\, R}{t^*}$$

$$\sigma_{\text{axial}} = \frac{P\, R}{2\, t^*}$$

Von Mises stress is then:

$$\sigma_{\text{VM}} = \sqrt{{\sigma_{\text{hoop}}}^2 - \sigma_{\text{hoop}}\, \sigma_{\text{axial}} + {\sigma_{\text{axial}}}^2}$$

### *3.6.7 Scripting & Plots*

These equations have been scripted in python and optimized using swept parameters to find the best printable isogrid density, pattern & flange cross section. The optimizer uses a 50-bar pressure load and RPA Thermal data as the load case to optimize the isogrid, as 40 Bar is the 2x Safety factor of the nominal chamber pressure and the Δp across the chamber and the coolant channels is 50-bar, hence 50-bar would be acting on the outer wall inside the cooling channels

The optimized results can be found below:

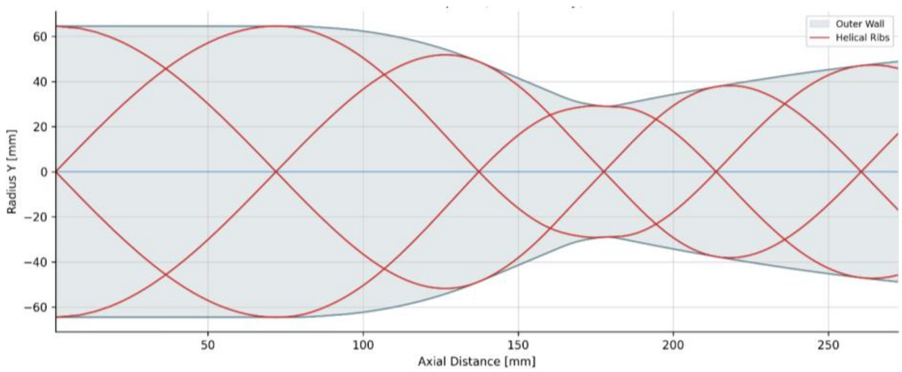


*Figure 15 – 2D View of Optimised Isogrid Helices*

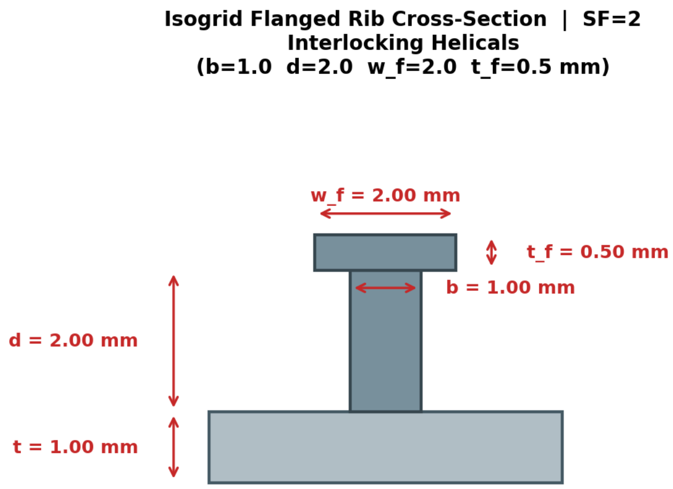


*Figure 16 – Cross section of Optimised Isogrid T-Flange*

#### *3.6.8 Finite Element Analysis Correlation*

##### *3.6.8.1 Plain Outer Wall Analysis*

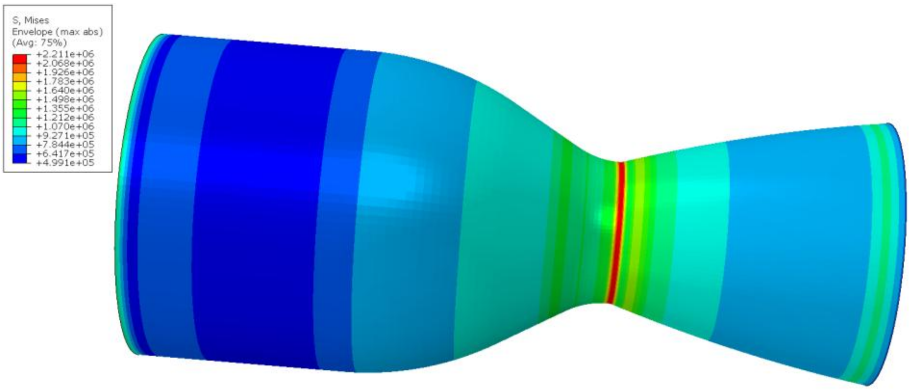


*Figure 17 – Plain Outer Wall Von Mises plot in KPa (Subjected to Thermal + Pressure Loading)*

Figure 21 shows the bare 1 mm outer wall under combined thermal and 49 bar pressure loading, with peak Von Mises values of ~2.2 **GPa** localised at the throat, which is to be thickened locally. Away from the throat the stress field is essentially uniform at approximately $\sigma_{\mathrm{VM}}$ = **1 GPa**, dominated by the restrained membrane thermal stress.

Using $\sigma_{\mathrm{yield}}(T_{\mathrm{wc}}(x))$ of 1100MPa (at 473K, the max operating temp relative to the outer wall)

$$SF(x) \; = \frac{\sigma_{\mathrm{yield}}(T_{\mathrm{wc}}(x))}{\sigma_{\mathrm{VM}}(x)} = 1.1$$

An SF of 1.1 on the plain outer wall leaves effectively zero margin against yield if operated at 40-Bar chamber pressure, which motivates the isogrid reinforcement to recover the SF ≥ 2 design target.

##### *3.6.8.2 Plain Outer Wall Analysis*

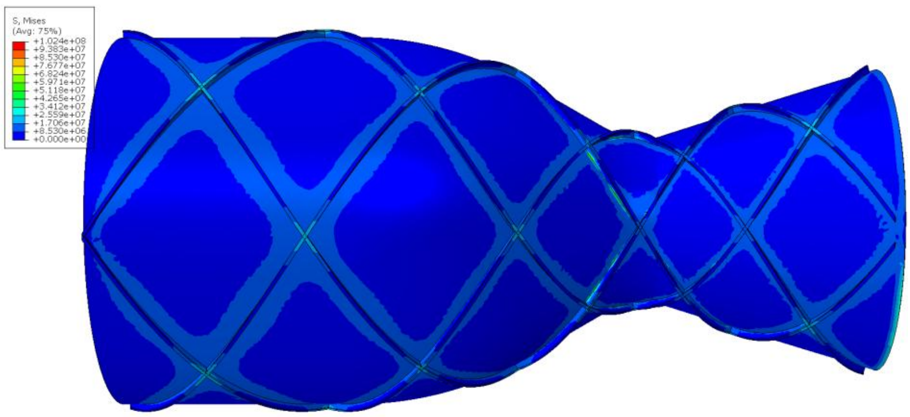


*Figure 18 – Outer Wall with Isogrid Von Mises plot in Pa (Subjected to Thermal + Pressure Loading)*

Figure 22 shows the same load case applied as Figure 21 to the isogrid-reinforced outer wall. The Interlocking Helices lattice drops the global average Von Mises to approximately $\sigma_{\mathrm{VM}}$ = **450 MPa**, a ~2.5× reduction compared to the plain shell, because the ribs carry the hoop and axial load paths in parallel with the skin and reduce the membrane stress in both families. The rib-intersection nodes remain well below yield, there is a max Von Mises (Red to Yellow Contours) shown in Figure 22 at **1GPa – 500MPa**, this is due to a mesh-quality artifact and is to be taken as an artificial spike in Von Mises.

Using $\sigma_{\mathrm{yield}}(T_{\mathrm{wc}}(x))$ of 1100MPa (at 473K, the max operating temp relative to the outer wall)

$$SF(x) = \frac{\sigma_{\mathrm{yield}}(T_{\mathrm{wc}}(x))}{\sigma_{\mathrm{VM}}(x)} = 2.4$$

This correlates to the optimiser's predicted SF of 2 closely because the Interlocking Helices lattice. The small residual difference between the analytical SF=2 target and the FEA SF=2.4 reading is the expected margin: the NASA-handbook smeared model assumes a perfectly periodic rib distribution, whereas the discrete FEA mesh captures the real load-sharing at each rib intersection and the slightly-non-uniform temperature field, both of which act conservatively in favour of the structure. The agreement within ~20 % confirms the smeared optimiser is a valid first-pass sizing tool for the Interlocking Helices pattern, and the FEA simply refines the prediction by a small margin without invalidating the design point.

## B3.7 – Simulating Exhaust Flow (STAR-CCM)

As a step towards accurately modelling rocket thrust chambers, the engine 1 hot fire was simulated using STAR-CCM, shown in Figure 19.

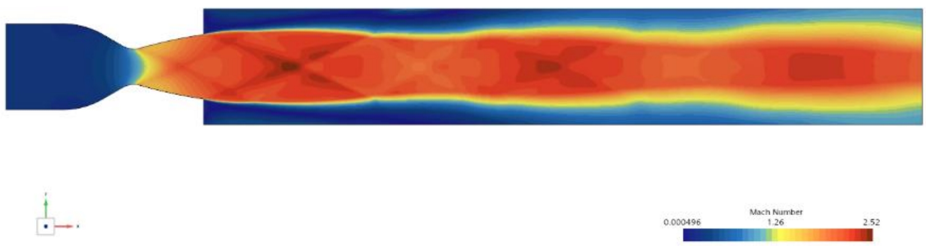


*Figure 19: A simulation of the nozzle and exhaust of an engine 1 hot fire.*

This 2D simulation uses the k-epsilon physics model for turbulent flow conditions. The chamber uses trimmer meshing with a 0.001m base size and 10 prism layers at the walls to accurately capture fluid flow at the boundary. The chamber entrance is modelled as a stagnation inlet with a 20-bar output pressure. Figure 19 shows the resulting Mach numbers across the chamber and the wake. As expected, the fluid is accelerated to Mach 1 at the throat and produces the characteristic shock diamonds in the exhaust. In future, we aim to improve these models by introducing thermal boundary conditions for conjugate heat transfer analysis.

## B3.7 – Engine 1

"Engine-1" is a completed and manufactured engine that shall act as the 'backup' for the newly designed engine in the event it is not manufactured by the necessary deadline(s). It is a simple regeneratively cooled straight channel engine. The details of this engine are listed in the figures (**Error! Reference source not found.**, **Error! Reference source not found.**) and tables (**Error! Reference source not found.**, **Error! Reference source not found.**) below.

*Table 11: Engine-1 dimensions*

| Property | Value |
|---|---|
| Engine length | 275.0mm |
| L* | 843.4mm |
| Chamber diameter | 118.9mm |
| Throat diameter | 48.54mm |
| Expansion area ratio | 3.36 |
| Contraction area ratio | 6.00 |

*Figure 20: 3/4 Section of Engine-1*

*Figure 21: 1/2 section view of Engine-1 & regenerative cooling channel profile*

*Table 12: Engine-1 cooling channel dimensions*

| Property | Value | Units |
|---|---|---|
| Wall thickness | 0.8 | $mm$ |
| Number of cooling channels | 56 | [-] |
| Rib thickness 'b' *(Chamber - Throat - Manifold)* | 2.80 – 0.86 – 2.00 | $mm$ |
| Channel width 'a' *(Chamber - Throat - Manifold)* | 4.00 – 2.00 – 3.00 | $mm$ |
| Channel height 'hc' *(Chamber - Throat - Manifold)* | 1.50 – 2.00 – 1.50 | $mm$ |
| Channel angle | 0 | ° |

### Engine-1

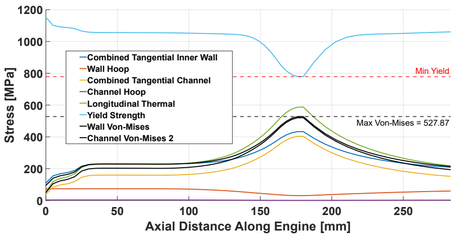


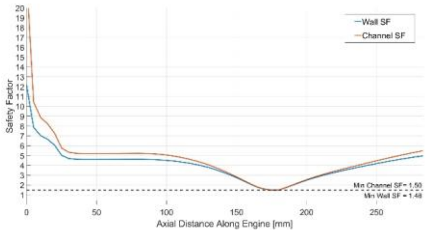


| Property | Value |
|---|---|
| Minimum wall safety factor | 1.48 |
| Minimum channel safety factor | 1.50 |
| Maximum von-Mises stress | 527.87 $MPa$ |

### Engine-1

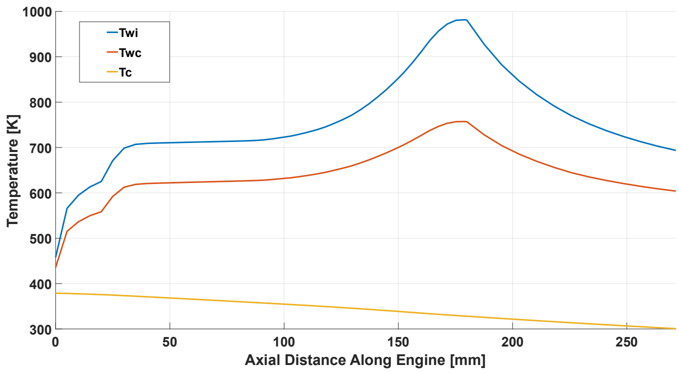


*Figure 22: Engine 1 temperature profile (without PDMS)*

*Table 13: Key thermal values for Engine-1*

| Property | Value | Units |
|---|---|---|
| Maximum chamber-side wall temperature | 982 | $K$ |
| Maximum coolant-side wall temperature | 757 | $K$ |
| Maximum coolant temperature | 378 | $K$ |
| Minimum velocity of coolant | 3.62 | $ms^{-1}$ |
| Maximum heat flux | 5047 | $kWm^{-2}$ |
| Increase in coolant temperature | 80 | $K$ |

## B3.8 – PDMS Ablative

PDMS reduces the total heat flux across the entire engine by creating silicon dioxide upon combustion which is deposited along the engine's inner walls and acts as an ablative thermal coating. At 2% PDMS, the expected heat flux reductions are within the range of 25-60% with negligible effects on the performance of the engine. When used in preliminary RPA simulations the PDMS additive will be modelled in the thermal analysis of the combustion chamber as approximately a 20% reduction in total heat flux at the throat. This will act as a conservative thermal estimate and may not accurately represent the potential heat flux reductions elsewhere in the engine.

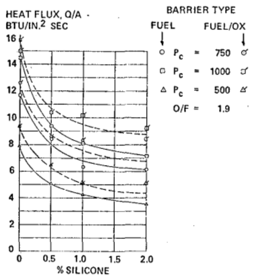


*Figure 23: Heat flux reduction as a function of PDMS addition*